Linear Dynamics of Transient Planetary Waves in the Presence of Damping†

B. WANG

Geophysics Fluid Dynamics Program, Princeton University, Princeton, NJ 08540

A. BARCILON

Geophysical Fluid Dynamics Institute and Department of Meteorology, Florida State University, Tallahassee, FL 32306

L. N. HOWARD

Department of Mathematics, Florida State University, Tallahassee, FL 32306

(Manuscript received 28 September 1984, in final form 2 April 1985)

ABSTRACT

The model presented here extends the Charney model by including Newtonian cooling, Ekman dissipation, and a linear vertical variation of the stratification parameter. By using an integral representation of the solution and a Frobenius series expansion, we have shown that the dispersion equation and the vertical structure of the strongly unstable modes can be well approximated by a second-order transcendental equation and a generalized Laguerre polynomial multiplied by an exponential function, respectively.

The midlatitude planetary wave 2, 3 and 4 belong to the intermediate scale motion between the Charney and Burger regimes, and may be viewed as the atmospheric counterpart of the most unstable Green mode. The wavelength (growth rate) ratio of the most unstable Green mode to most unstable Charney mode is about 2.5 to 3 (1/3 to 2/5) for typical midlatitude winter condition. That mode possesses a constant phase which tilts westward with height in the troposphere, and features a barotropic structure in the stratosphere; that mode extends to several density heights before being trapped, and exhibits a major peak in the stratosphere. Its available potential energy is converted in the lower troposphere, as well as in the stratosphere, and its kinetic energy is generated in both the middle troposphere and the middle stratosphere, with significant destruction near the tropopause.

The Newtonian cooling was found to reduce the growth rate over most of the wavelength band especially for the Burger-Green modes and for the strong instabilities. Nevertheless, in the immediate vicinity of the critical wavelength small amount of Newtonian cooling has a destabilizing effect. The vertical increase of the static stability reduces the wavelength of the most unstable modes and affects the growth rate and vertical structure of the Green modes.

1. Introduction

Although the planetary waves display a quasi-stationary character, in part due to mechanical and thermal forcings (Perry, 1967; Holton, 1975) mainly found in the Northern Hemisphere where topography and land–sea heat contrasts are significant, there nevertheless exists well documented evidence that the winter circulation, especially in the Southern Hemisphere, features transient planetary waves characterized by: 1) a slow eastward propagation of a few meters per second in excess of the zonally averaged surface wind speed; 2) a westward tilt with height of the constant phase line, especially in the troposphere, but not in the middle stratosphere; 3) a maximum wave amplitude in the stratosphere (Philpot, 1969; Hartmann, 1976; Leovy and Webster, 1976; Mechoso and Hartmann, 1982). These observations suggest that the generating mechanisms of these eastward propagating planetary waves differ from those responsible for the quasi-stationary waves and suggest a genesis rooted in a baroclinic instability mechanism.

The slowly growing modes found in the longer wavelength bands were first found by Green (1960) who calculated their growth rate to be an order of magnitude smaller than those of the Charney modes. Although discounted at first, the practical importance of the slowly growing Green modes emerged as evidence of transient planetary waves became available. Recent numerical studies of baroclinic instability of the more realistic atmospheric zonal flows at planetary wave scale (Geisler and Garcia, 1977; Kuo, 1979; Fullmer, 1982) showed that, in the absence of dissipation, the Green modes have moderately short doubling time (~1 week)

† Contribution No. 220 of the Geophysical Fluid Dynamics Institute, Florida State University.

and exhibit a streamfunction having an oscillating amplitude that extends to the stratosphere where it is considerably larger than at the ground.

Quasi-geostrophic motion (Rossby number Ro $\ll 1$) may be classified into two categories (Phillips, 1963): 1) $L/R_a \ll 1$; 2) $L/R_a \sim 1$ (Burger, 1958), where R_a is the radius of the Earth. The first kind of geostrophic motion, which is referred as the Charney regime, has a characteristic length scale comparable to the Rossby radius of deformation, L_D; for midlatitude atmospheric motions $L_D \sim 10^3$ km, corresponding to the cyclone wave scale. Midlatitude planetary waves have characteristic x-scales which are about 2.5 to 3 times larger than L_D, and Gent (1974) showed how the meridional shear confines these waves in the north–south direction. If we choose two latitudes such that the zonal velocity at these latitudes is one third of its maximum value in the westerlies, we find that, in the winter of the Northern Hemisphere, the width, L_y, of the westerlies centered about the latitude θ_0 ($\sim$40°N) is around 5000 km. We will take the characteristic length scale L to be half that value so that $4L$ is representative of the x-wavelength for the planetary waves 2, 3 and 4 but not for wave 1. The latter belongs to the second kind of quasi-geostrophic motions, which is referred to as the Burger regime. Since $L_D < L < L_\beta$, where $L_\beta = R_a \text{cotan}\theta_0$, we conclude that the motions for waves 2, 3 and 4 are characterized by the so-called "intermediate" scale (Charney and Flierl, 1981). Then, if $V \sim 10$ m s^{-1}, we find that $R_0 \sim 0.045$ and $L/L_\beta \sim 0.3$, the smallness of this last ratio justifying the use of the β-plane approximation (Appendix B, lists the symbols used in this paper).

Although R_0, L/L_β are small for both cyclone and planetary waves, the inverse Burger number, $S^{-1} = L^2/L_D^2$, and the β-parameter, $L/(L_\beta R_0)$, are O(1) for cyclone waves but much larger than unity ($\sim$10) for planetary waves. Because of their horizontal extent, we anticipate that planetary waves will reach to great heights and that the vertical variations of density and static stability will play an important part in their dynamics. These waves are also characterized by long time scales, and diabatic heating and boundary layer dissipation must be included in the model. As has been discussed by Wiin-Nielsen (1975), the major diabatic heating for the large scale, quasi-geostrophic, linear motion may be expressed in terms of Newtonian cooling form. We shall consider the Newtonian cooling as a representative diabatic heating process.

Based on the above considerations we propose, in this paper, to extend the Charney (1947) model by including: 1) Newtonian cooling, 2) a linear variation of N^2 with z, and 3) Ekman layer dissipation.

Charney (1947) obtained solutions of his model in terms of hypergeometric functions; the complication of these functions made numerical computations necessary and slowed down analytical extensions of his model. Although some efforts were made to simplify the exact solutions by Lindzen and Rosenthal (1981), who used a WKB asymptotic analysis, and by Branscome (1983), who used a short-wave expansion and expansions near the critical neutral points, the effects of Newtonian cooling were mostly studied analytically within the context of the much simpler two-layer or Eady models. The conclusions derived from these models may be questioned because of their limitations. Furthermore, in order to understand what physical factors control or affect the dynamics of the unstable waves, it is desirable to obtain a more tractable representation of the solution. In what follows we strive to obtain simplified, yet accurate expressions for the dispersion relation and the eigenfunctions for the generalized Charney instability problem.

Our investigation will focus on:

1) the wave selection mechanism, especially in the planetary wave band, and on the role played by the linear increase with height of the stability parameter;

2) the effects of Newtonian cooling and Ekman layer dissipation on the phase speed and growth rate as well as on the vertical structure of the planetary waves;

3) the vertical structure and the energy conversions for the strongly unstable Green modes; comparison will be made with the corresponding quantities of the Charney modes.

The present investigations of both planetary and cyclone waves will serve as a prelude to the study of the nonlinear dynamics of planetary waves in the presence of Newtonian cooling and Ekman dissipation (Wang and Barcilon, 1985).

2. Dynamic equations

Our governing equation is the diabatic quasi-geostrophic potential vorticity equation which we write for a non-Boussinesq fluid having a constant scale height, $H = RT_0/g$, in the $z_* = -H \ln p/p_0$ coordinate on a midlatitude β-plane. The nondimensional governing equation is equivalent to that found in Pedlosky (1979) if we take the basic state density as $\rho_s = \rho_0 \times \exp[-(D/H)z]$ in his equation (6.5.18). When multiplied by the Burger number $S = L_D^2/L^2$ that equation takes the form

$$\left(\frac{\partial}{\partial t} + \frac{\partial \psi}{\partial x}\frac{\partial}{\partial y} - \frac{\partial \psi}{\partial y}\frac{\partial}{\partial x}\right) \times \left[S\nabla^2\psi + S\beta y + N^2\frac{\partial}{\partial z}\left(N^{-2}\frac{\partial \psi}{\partial z}\right) - \frac{D}{H}\frac{\partial \psi}{\partial z}\right] = N^2\frac{\partial}{\partial z}(N^{-2}\dot{Q}) - \frac{D}{H}\dot{Q}; \quad (2.1)$$

the boundary conditions are

$$\frac{\partial \psi}{\partial x} = 0 \quad \text{at} \quad y = \pm 1, \quad (2.2)$$

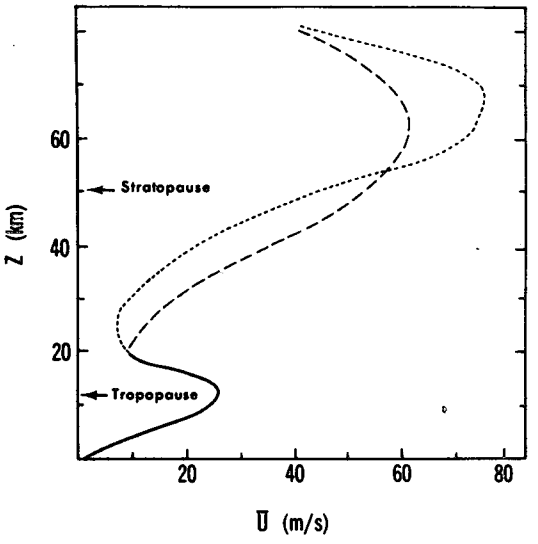

FIG. 1a. Vertical variations of zonally averaged mean current for the westerlies of Northern Hemisphere. Solid, dashed and dotted lines are based on the data from Oort and Rasmusson (1974), Wallace and Hobbs (1977), and Palmen and Newton (1969), respectively.

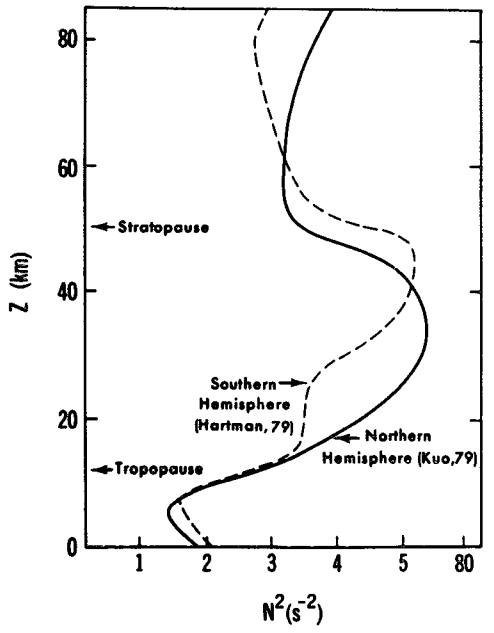

FIG. 1b. Variations of Brunt-Väisälä frequency squared, N^2 with height for the Westerlies of Northern (solid line) and Southern (dashed line) hemisphere during the winter season. Northern and Southern Hemisphere data were adapted from Kuo (1979) and Hartmann (1979), respectively.

and, at the ground $z = 0$,

$$\frac{\partial^2\psi}{\partial t\partial z} + \frac{\partial\psi}{\partial x}\frac{\partial^2\psi}{\partial y\partial z} - \frac{\partial\psi}{\partial y}\frac{\partial^2\psi}{\partial x\partial z} + \frac{S}{2\,\mathrm{Ro}}\left(\frac{De}{D}\right)\nabla^2\psi - \dot{Q} = 0, \quad (2.3)$$

with the additional requirement that the flux of energy vanishes as $z \to \infty$. In these equations we scaled (x, y) by L, z_* by D, time t by the advective time scale L/V, the geostrophic streamfunction ψ by LV and the diabatic heating rate, Q_*, by $(H/D)f_0V^2C_P/R$ where R is the gas constant and C_P the specific heat at constant pressure; $N = (gd\ \ln\theta_s/dz)^{1/2}$ is the Brunt-Väisälä frequency; $\mathrm{Ro} = (V/f_0L)$ the Rossby number; $\beta = \beta_0L^2/V$ denotes the nondimensional β-parameter, where $\beta_0 \equiv 2\Omega \times \cos\theta_0/Ra$ is the meridional gradient of the Coriolis parameter; $D_e = (2A_z/f_0)^{1/2}$ is a measure of the Ekman layer depth, where A_z is an eddy kinematic viscosity coefficient.

We will focus on the stability of baroclinic flows, i.e., we write

$$\psi = -yU(z) + \phi(x, y, z, t) \quad (2.4)$$

where $\phi(x, y, z, t)$ is the perturbation. As seen from Fig. 1a, below 70 km the zonally averaged flow in the winter can be approximated reasonably well by a constant vertical shear, though there is an internal jet near the tropopause. Kuo's (1979) results suggest that the sharp change in the zonal flow profile near that level does not alter the qualitative picture of the instability. We then choose the nondimensional velocity scale as $V = \lambda_* D$, λ_* being the dimensional shear, and confine our analysis to

$$U(z) = z. \quad (2.5a)$$

The assumption that N^2 is a linearly increasing function of z is a crude approximation. The fact that in our model N^2 increase with height as z increases can be justified as follows. The Charney and Green modes have their turning points in the troposphere and stratosphere, respectively, i.e., above these heights these modes exhibit exponential decay and are not much affected by the detailed structure of the basic state. This is, in part, the motivation for choosing

$$N^2 = N_0^2(1 + \hat{\alpha}z) \quad (2.5b)$$

where N_0^2 is a constant and $\hat{\alpha} \sim O(10^{-1})$. Another motivation for such a choice can be found if we consider the static balance of a model, perfect gas atmosphere with a constant but small lapse rate. The resulting expression for N^2 can then be approximated by a linear variation with z. This choice for N^2 does not possess a sharp discontinuity at the model tropopause. (Here we will use the terms troposphere and stratosphere to denote the range of heights typically associated with these regions.) We conjecture that because we are dealing with planetary waves of great vertical extent, the existence of a sharp change in static stability near the tropopause will not have an appreciable effect on their dynamics, but the slow change of N^2 over great heights will. This conjecture will be checked *a posteriori* by comparing some of our findings with numerical calculations by Geisler and Garcia (1977) who used realistic static stability profiles. Also, it should be noted that Grotjahn (1980), in his study on the ef-

fects of the tropopause on the linear dynamics, found that, in general, the solutions are sensitive to changes in the tropopause structure only when they have large amplitudes in the vicinity of that level or when the forcing is significantly altered by the tropopause structure. We will show that the Green modes, which are free modes, usually attain their minimum amplitude at the tropopause.

Finally, we model the diabatic rate of heating by means of a Newtonian cooling,

$$\dot{Q} = -\mu \frac{\partial \phi}{\partial z} \tag{2.5c}$$

where $\mu = L/V\tau_*$ is the nondimensional Newtonian cooling coefficient and τ_* is the dimensional Newtonian cooling time. For details the reader is referred to Wang (1984).

After using (2.4), (2.5a), (2.5b) and (2.5c) in our governing system of equation and boundary conditions and neglecting $O(\hat{\alpha}^2)$ terms we arrive at

$$\left(\frac{\partial}{\partial t} + z\frac{\partial}{\partial x} + J(\phi, \quad)\right)\left[S_0\nabla^2\phi + \frac{\partial^2\phi}{\partial z^2} - \alpha\frac{\partial\phi}{\partial z}\right] + b\frac{\partial\phi}{\partial x} + \mu\left(\frac{\partial^2\phi}{\partial z^2} - \alpha\frac{\partial\phi}{\partial z}\right) = 0 \tag{2.6}$$

with, at $z = 0$,

$$\left(\frac{\partial}{\partial t} + J(\phi, \quad)\right)\frac{\partial\phi}{\partial z} - \frac{\partial\phi}{\partial x} + \delta\nabla^2\phi + \mu\frac{\partial\phi}{\partial z} = 0, \tag{2.7}$$

and, as $z \to \infty$, the upward energy flux vanishes, i.e.,

$$\lim_{z\to\infty} \overline{\rho_s\phi\left[\left(\frac{\partial}{\partial t} + z\frac{\partial}{\partial x} + J(\phi, \quad)\right)\frac{\partial\phi}{\partial z} - \frac{\partial\phi}{\partial x} + \mu\frac{\partial\phi}{\partial z}\right]} = 0, \tag{2.8}$$

and, at $y = \pm 1$,

$$\frac{\partial\phi}{\partial x} = 0. \tag{2.9}$$

In these equations

$$\alpha = \frac{D}{H} + \hat{\alpha}, \tag{2.10a}$$

$$b = \alpha + \frac{1}{\lambda} + \frac{\hat{\alpha}}{\lambda}z + O(\hat{\alpha}^2 z) \tag{2.10b}$$

$$\lambda \equiv \lambda_*/(\beta_0 N_0^2 D/f_0^2) \tag{2.10c}$$

$$S_0 \equiv \frac{N_0^2 D^2}{f_0^2 L^2} \tag{2.10d}$$

$$\delta = \frac{N_0^2 D_e}{2f_0 L\lambda_*}. \tag{2.10e}$$

The quantity α reflects the combination of effects of mass convergence (D/H) and linear increase of N^2 through $\hat{\alpha}$. Nondimensional shear λ measures the competitive effects of the baroclinic vortex stretching vs the β-effect in producing potential vorticity and constitutes one of the fundamental parameters in this problem. The quantity b is proportional to the basic state north–south potential vorticity gradient, while μ and δ are measures of the Newtonian cooling and the Ekman layer dissipation, respectively. The Jacobian

$$J(A, B) \equiv \frac{\partial A}{\partial x}\frac{\partial B}{\partial y} - \frac{\partial A}{\partial y}\frac{\partial B}{\partial x}$$

denotes nonlinear terms and will be neglected in this paper but retained in the weakly nonlinear analysis of Wang and Barcilon (1985) that builds upon this work.

The linearized version of Eq. (2.6) reduces to the Charney (1947) problem if $\hat{\alpha} = \mu = \delta = 0$, and to Burger's (1958) equation if $\hat{\alpha} = \mu = \delta = 0$ and if we neglect $S_0\nabla^2\phi$ compared to $\partial^2\phi/\partial z^2 - \alpha(\partial\phi/\partial z)$. For waves 2 and 3 we estimate that $S_0\nabla^2 \sim K^2 S_0 \sim 0.5$, 0.7 respectively which are not small enough to be neglected. Here K is the total horizontal wavenumber. If $S_0\nabla^2$ were neglected, not only would we underestimate the role of the meridional scale and distort the vertical structure of the unstable waves, but we would alter appreciably the planetary wave selection mechanism.

The quantity D/H in (2.10a) serves as a tracer of the mass convergent effect; as $D/H = 0$, we recover the Boussinesq approximation. In what follows we will consider the non-Boussinesq case (set $D = H$) and discuss only the Boussinesq results to contrast these with the non-Boussinesq findings.

3. Exact and approximate normal mode solutions

Let

$$\phi(x, y, z, t) = e^{\alpha z/2}\Phi(z)e^{ik(x-ct)}\cos ly + \text{c.c.} \tag{3.1}$$

where $l = (m + \frac{1}{2})\pi$, $m = 0, 1, 2, \cdots$ and c.c. denotes complex conjugate. Using (3.1) in the linearized version of (2.6), transforming the independent variable z to ξ, we find that the eigenfunction $\Phi(\xi)$ satisfies

$$\xi\frac{d^2\Phi}{d\xi^2} + (\eta - \xi)\Phi = 0 \tag{3.2a}$$

with, at $\xi = -\sigma$,

$$\sigma\left(\frac{d\Phi}{d\xi} + \frac{\alpha}{2\tilde{K}}\Phi\right) + \left(1 - i\delta\frac{K^2}{k}\right)\Phi = 0 \tag{3.2b}$$

and, as $\xi \to \infty$,

$$\Phi e^{(\alpha/2\tilde{K})\xi} \tag{3.2c}$$

remains bounded. The unfamiliar reader is referred to Pedlosky (1979, Section 7.8) for the details of the derivation of an equation similar to (3.2a). In (3.2),

$$\xi = \tilde{K}z - \sigma \tag{3.3a}$$

is the transformed independent variable, where

$$\tilde{K} = \left[S_0 K^2 + \frac{\alpha^2}{4} - \frac{\hat{\alpha}}{\lambda} \right]^{1/2}, \quad (K^2 = k^2 + l^2) \tag{3.3b}$$

is the total wavenumber scaled by L_D^{-1} for the Boussinesq fluid ($\alpha = \hat{\alpha} = 0$), and will be referred as the modified total wavenumber,

$$\sigma = \tilde{K}(c + i\mu k^{-1}) \tag{3.3c}$$

is the eigenvalue proportional to complex phase speed c in the absence of Newtonian cooling. The only parameter entering (3.2a) is

$$\eta = \frac{1}{\tilde{K}} \left(\alpha + \frac{1}{\lambda} + \frac{\hat{\alpha}\sigma}{\lambda \tilde{K}} - iS_0 \mu \frac{K^2}{k} \right); \tag{3.3d}$$

in the absence of Newtonian cooling, $\mu = 0$, and variations of N^2, $\hat{\alpha} = 0$, and $\alpha = 1$. Equation (3.3d) denotes the basic state potential vorticity gradient divided by the modified total wavenumber. The last two terms of (3.3d) are much smaller than the first two terms which are O(1), since $\hat{\alpha}$, S_0, σ, μ are all small, in general. Because of its inverse dependence on $\tilde{K}$, loosely speaking, for a given basic state, η may be viewed as a quantity proportional to the wavelength.

Note that, from (3.3d), the quantity η depends on the eigenvalue σ via the small term $\hat{\alpha}\sigma/\lambda\tilde{K}^2$. In what follows, we will formally derive the dispersion relation for σ. We will then approximate η by an expression independent of σ, as done in (4.3). The validity of this approximation is displayed graphically (in Fig. 5) and will be discussed later.

If $\Phi_1(\xi)$, $\Phi_2(\xi)$ are two linearly independent solutions of (3.2a) we can write the general solution for Φ as

$$\Phi(\xi, \eta) = \mathcal{C}_1(\eta)\Phi_1(\xi) + \mathcal{C}_2(\eta)\Phi_2(\xi) \tag{3.4}$$

where $\mathcal{C}_1(\eta)$ and $\mathcal{C}_2(\eta)$ must be chosen so as to satisfy the upper boundary condition and are given below. Since $\xi = 0$ is a regular singular point of the governing equation, we use Frobenius power series expansions to obtain $\Phi_1(\xi)$ and $\Phi_2(\xi)$ (see Appendix A) and we render the logarithm single valued by choosing the branch cut such that

$$\ln\xi = \ln|\xi| + i \arg\xi, \quad -\pi < \arg\xi \leqslant \pi.$$

Appendix A gives

$$\mathcal{C}_2(\eta) = (e^{i\pi\eta} - 1)/2\pi i,$$

$$\mathcal{C}_1(\eta) = \mathcal{C}_2(\eta) f(\eta), \tag{3.5}$$

where

$$f(\eta) = \ln 2 - 1 + 2\gamma + \frac{1}{\eta} + \psi\left(\frac{\eta}{2}\right) + \pi \cot\left(\frac{\pi\eta}{2}\right), \tag{3.6}$$

and $\gamma = 0.57721\cdots$ is Euler's constant while $\psi(x)$ is the logarithmic derivative of the Gamma function. When $\eta = \eta_c = 2n$ where $n = 1, 2, \cdots$

$$\mathcal{C}_2(2n) = 0, \quad \mathcal{C}_1(2n) = 1, \tag{3.7}$$

and we get the neutral solution. We will call η_c the critical points. After substituting (3.4), into the lower boundary conditions, (3.2b), we obtain the dispersion relation which we express as

$$\lim_{J\to\infty} \left[\sum_{j=0}^{J} A_j \sigma^j + \sigma \ln(-\sigma) \sum_{j=0}^{J-1} B_j \sigma^j \right] = 0, \tag{3.8}$$

where

$$A_0 = \mathcal{C}_2 b_0 (1 - i\delta K^2 k^{-1}),$$

$$A_1 = \mathcal{C}_2(a_1 + \nu b_0) + i\mathcal{C}_1 a_1 \delta K^2 k^{-1}.$$

$$A_j = (-1)^j \{ \mathcal{C}_1 [a_j (1 - j - i\delta K^2 k^{-1}) - \nu a_{j-1}] + \mathcal{C}_2 [-a_j - \nu b_{j-1} + (1 - j + i\delta K^2 k^{-1}) b_j] \}, \quad j \geqslant 2, \tag{3.9}$$

$$B_0 = i\mathcal{C}_2 \delta K^2 k^{-1},$$

$$B_j = (-1)^j \mathcal{C}_2 [(j + i\delta K^2 k^{-1}) a_{j+1} + \nu a_j], \quad j \geqslant 1,$$

a_j and b_j being given in Appendix A. In principle, from (3.8) we calculate the complex phase speed,

$$c = c(\tilde{K}; \lambda, \mu, \delta, \alpha).$$

To obtain simpler, approximate and more meaningful expressions for the dispersion relation (3.8), and to test the accuracy of these approximations, we recover the Charney problem by setting $\hat{\alpha} = \mu = \delta = 0$, and we truncate (3.9) by taking $J = 10, 3, 2$; we refer to these truncated expressions as the tenth-, third- and second-order dispersion relations, respectively. Figure 2 shows plots of σ versus η obtained from these approximations. The differences between values of σ obtained from the tenth- and third-order truncations are very small for most of values of η. Also, the second-order truncation yields accurate results near the critical points η_c, but the errors become slightly larger when the most unstable modes are considered.

In view of the preceding, for a local analysis near the critical points, we use the second-order dispersion relation obtained from (3.8),

$$-\frac{1}{\eta} + \left(1 - \frac{\nu}{\eta}\right)\sigma + \left[\left(\frac{1}{2\eta} - \frac{\eta}{4} \right) + f(\eta) \left(\frac{\eta}{2} - \nu \right) \right] \sigma^2 + \left(\frac{\eta}{2} - \nu \right) \sigma^2 \ln(-\sigma) + i\delta K^2 k^{-1} \left\{ \frac{1}{\eta} + \sigma f(\eta) + \sigma \ln(-\sigma) + \frac{\eta}{2} \sigma^2 \ln(-\sigma) + \left[\frac{\eta}{2} f(\eta) + \frac{1}{4\eta} (3\eta^2 - 2) \right] \sigma^2 \right\} = 0 \tag{3.10}$$

where

$$\nu \equiv \alpha/2\tilde{K} \tag{3.10a}$$

and $f(\eta)$ is given by (3.6). It can be shown that (3.10) filters out the westward moving neutral modes i.e., the

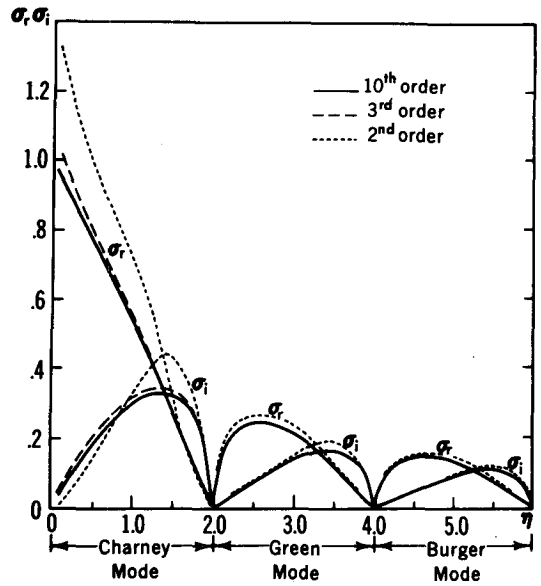

FIG. 2. Eigenvalue $\sigma = \tilde{K}c$ as a function of parameter $\eta = (1 + \lambda^{-1})/\tilde{K}$ (approximately proportional to wavelength) for a non-Boussinesq fluid. The solid, dashed, and dotted lines represent the results calculated from tenth-, third-, and second-order truncated dispersion relations, respectively. For the Green and Burger modes the tenth- and third-order dispersion equation give the same curves.

Rossby waves, and thus retains the relevant physics as far as the instability problem is concerned. Equation (3.10) can be simplified further if we multiply it by ϵ and write

$$\eta = \eta_c + 2\epsilon. \tag{3.11}$$

Furthermore, we assume $|\epsilon|$ to be small so that $|\sigma| \ll 1$. After neglecting terms whose order is higher than $O(\sigma^4, \epsilon\sigma^2)$ we find that, in the vicinity of the critical points $\eta_c = 2n$, the second-order dispersion relation takes the form

$$(n-\nu)\sigma^2 + \left(1 - \frac{\nu}{2n}\right)\epsilon\sigma - \frac{\epsilon}{2n} + (n-\nu)\epsilon\sigma^2 \ln(-\sigma) + i\delta\frac{K^2}{k}\left[\frac{\epsilon}{2n} + \sigma + n\sigma^2 + \epsilon(1+n\sigma)\sigma\ln(-\sigma)\right] = 0. \tag{3.12}$$

The vertical structure of the unstable modes is given by

$$\tilde{\Phi}(z) = e^{(\alpha/2)z}\Phi(z) = e^{(\alpha/2)z}[\mathcal{C}_1(\eta)\Phi_1(\xi) + \mathcal{C}_2(\eta)\Phi_2(\xi)]. \tag{3.13}$$

To obtain an approximate expression for $\tilde{\Phi}(z)$, we use (3.11) and expand $\Phi_1, \Phi_2, \mathcal{C}_1, \mathcal{C}_2$ in powers of ϵ. After some algebra (Wang, 1984) we obtain

$$\tilde{\Phi}(z; 2n + 2\epsilon) = \frac{\tilde{K}}{n} e^{pz + \tilde{K}(c - i\mu/k)}\left(z - c + i\frac{\mu}{k}\right) \mathcal{L}_{n-1}^{(1)}\left[2\tilde{K}\left(z - c + i\frac{\mu}{k}\right)\right] + O(\epsilon) \tag{3.14}$$

where

$$p \equiv \frac{\alpha}{2} - \tilde{K} < 0 \tag{3.15}$$

depicts the rate at which unstable wave amplitude decays with height, and

$$\mathcal{L}_m^{(l)}(x) \equiv \sum_{k=0}^{m} (-1)^k \binom{m+l}{m-k} \frac{x^k}{k!}$$

denotes the generalized Laguerre polynomial. For the Charney and Green modes, we take $n = 1$ and 2 respectively and get

$$\tilde{\Phi}(z; 2 + 2\epsilon) = \tilde{K}(z - c + i\mu k^{-1})e^{pz + \tilde{K}(c - i\mu k^{-1})} + O(\epsilon), \tag{3.16a}$$

$$\tilde{\Phi}(z; 4 + 2\epsilon) = \tilde{K}(z - c + i\mu k^{-1}) \times [1 - \tilde{K}(z - c + i\mu k^{-1})]e^{pz + \tilde{K}(c - i\mu k^{-1})} + O(\epsilon). \tag{3.16b}$$

4. Wave selection, strong and weak instabilities

We examine the wave selection mechanism first in an attempt to understand the role of the variations of N^2 with z and the role of the nondimensional shear when the dissipation mechanisms are absent, i.e. $\mu = \delta = 0$.

In Fig. 3a, b contours of $S^{1/2}Kc_I$, proportional to the growth rate, and of the phase speed, c_R, are displayed as functions of the nondimensional shear, λ, and the horizontal wavenumber squared, S_0K^2, these curves are calculated by the third order dispersion equation for $\hat{\alpha} = 0$. All wavenumbers grow except for the neutral modes found on critical curves $\eta = \eta_c$ which divide Fig. 3 into the Charney, Green, Burger regions; in each of these regions there is a narrow band of relatively large growth rate. We refer to the most unstable Charney and Green modes by MUCM, MUGM, respectively. The interesting feature is that (see Fig. 4) the loci of MUCM, MUGM are nearly parallel to the λ-axis, i.e., these regions of maximum growth rates are approximately described by $\eta = \eta_M$ = constant, where $\eta_M \approx 1.35$ and 3.35 for MUCM and MUGM, respectively. For the $\hat{\alpha} = 0$ case, the horizontal wavenumbers of the MUCM and MUGM depend only on the nondimensional shear, λ, i.e., using (3.3d) we get

$$S_0^{1/2}K = \frac{1}{\eta_M}\left[\left(1 - \frac{\eta_M^2}{4}\right) + \frac{2}{\lambda} + \frac{1}{\lambda^2}\right]^{1/2}, \tag{4.1}$$

and therefore,

$$\frac{K_{\text{MUCM}}}{K_{\text{MUGM}}} \approx 2.5\left[1 - \frac{9.2}{4\left(1 + \frac{1}{\lambda}\right)^2}\right]^{-1/2}, \tag{4.2}$$

where K_{MUCM}, K_{MUGM} are the total wavenumbers of these modes.

When $\hat{\alpha} \neq 0$, η becomes a weak function of the eigenvalue, σ, [see expression in (3.3d)] the coefficient of that quantity being a small number of $O(\hat{\alpha}/\lambda\tilde{K}^2)$. In

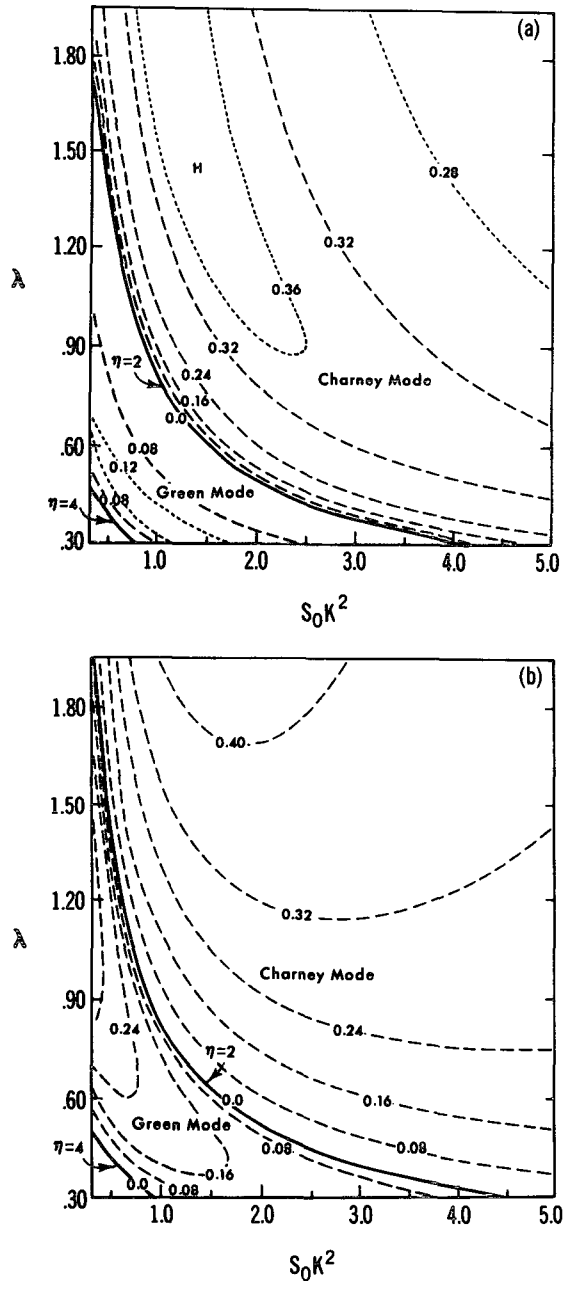

FIG. 3. (a) Growth rate $S_0^{1/2}Kc_I$ and (b) phase speed c_R given by third order dispersion relation for an inviscid non-Boussinesq fluid as a function of nondimensional shear λ and total wave number squared, $S_0K^2(\hat{\alpha} = 0)$. Solid lines are critical curves $\eta = 2$ and 4.

view of the smallness of that coefficient, a very useful approximation consists in dropping that term and writing

$$\eta \approx \frac{1}{K}\left(\alpha + \frac{1}{\lambda}\right); \tag{4.3}$$

Fig. 5 tests this approximation. It shows curves for c_I versus S_0K^2 in the absence of $\hat{\alpha}$ (solid line), when the full dependence on $\hat{\alpha}$ is retained (dashed line) and when the approximation (4.3) is made (dotted line). Thus, the validity of the above approximation is brought out graphically by comparing the dotted and dashed lines. The positions of the neutral and most unstable waves are practically unaffected by this approximation, c_I being slightly larger for the most unstable waves. Using (4.3) for $\eta = \eta_M$ we obtain

$$L_{\mathrm{MUM}} = 2\pi\eta_M\left[\frac{f_0^2\alpha^2}{N_0^2H^2}\left(1 - \frac{\eta_M^2}{4}\right) + \frac{\beta_0}{\lambda_* H}(2\alpha + \hat{\alpha}\eta_M^2) + \frac{N_0^2\beta_0^2}{\lambda_*^2 f_0^2}\right]^{-1/2}, \tag{4.4}$$

where we have assumed that the meridional wavenumber l is set to zero so that $k = K$. Table 1 shows the wavelengths for the most unstable Charney modes for the non-Boussinesq and the Boussinesq cases for various values of the dimensional shear, λ_*, latitude, θ_0, and $\hat{\alpha}$. We discuss these effects below.

As was shown by Held (1978), the vertical shear λ_* is one of the most important parameters in the wave selection. Figure 6 shows the sensitivity of the growth rate to changes in λ_*; plots of $S^{1/2}Kc_I$ versus S_0K^2 are displayed for two typical values of λ_*; $\lambda_* = 2.0 \times 10^{-3}$ s^{-1}, corresponding to tropospheric winter conditions, and $\lambda_* = 1.2 \times 10^{-3}$ s^{-1}, corresponding to a stratospheric layer. For large vertical shears, the wavelengths of both MUCM and MUGM shift to larger values. The ratio of the growth rate of MUGM to that of MUCM varies from about 1/3 to 2/5 with the shear decreasing from 2.4×10^{-3} s^{-1} to 1.4×10^{-3} s^{-1} near 40°N.

The variation in latitude θ_0 changes the value of β_0 and f_0 and therefore affects the scale, $\beta_0N_0^2D/f_0^2$, by which λ_* is nondimensionalized [see (2.10)]. The wavelengths of the most unstable modes increase with increasing latitude, implying that a faster rotation rate and a smaller β-effect ensure that the longer waves are selected as the most unstable waves. If we turn to Fig. 4a, we observe that the MUCM is found for large, while the MUGM is found for small λ. Therefore, given a value of λ_*, a smaller β-effect tends to increase the growth rate of the MUCM, while reducing that of the MUGM [recall (2.10c) and Fig. 4a].

When $\hat{\alpha} \neq 0$, the wavelengths for the MUCM become shorter as shown in Table 1. If we turn our attention to Fig. 6 and consider the shift in wavenumber for the Green modes we observe that the position of the MUGM when $\hat{\alpha} = 0$ almost coincides with the position of the *neutral* Green mode when $\hat{\alpha} = 0.1$; therefore, the changes due to the $\hat{\alpha}$-effect are more important at the ultralong wave band. The linear increase in N^2 corresponds, roughly, to the inclusion of the tropopause (see Green, 1960) and to that of the mass convergence effect (see Table 1). The Boussinesq approximation not only distorts the wave selection substantially, but also reduces the growth rate for most of the cyclone scale waves, by as much as 1/3 when $\lambda_* = 2.0 \times 10^{-3}$ s^{-1}.

Near the critical curves $\eta_c = 2n$, the growth rate increases much faster when $\eta < 2n$ than when $\eta > 2n$

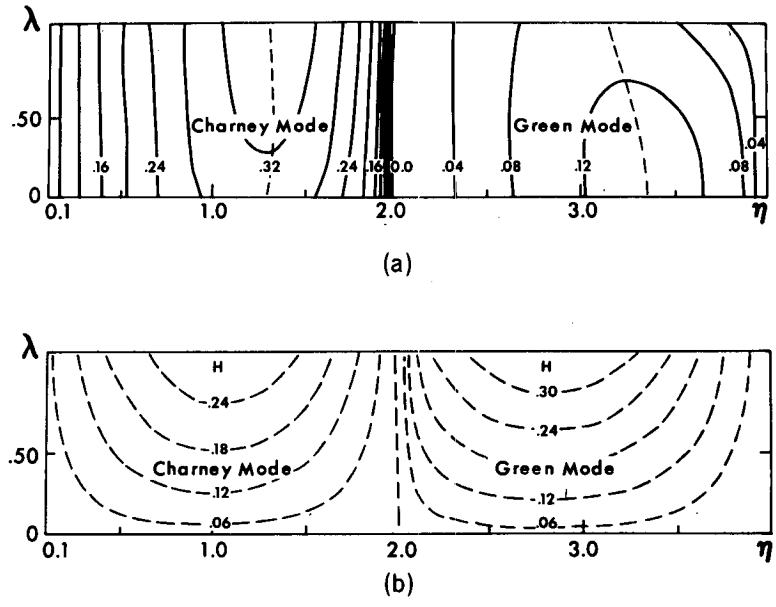

FIG. 4. As in Fig. 3 but as functions of parameter η and non-dimensional shear λ. Dashed lines in (a) show the loci of the most unstable Charney and Green modes.

(see Fig. 4a). If we let $\eta = 2n + 2\epsilon$, then $\epsilon = -0.1$ corresponds to an unstable mode with a growth rate 2/3 that of the corresponding most unstable mode. We refer to the instability for which $\epsilon < 0 (\epsilon > 0)$ as the strong (weak) instability. For the strong instability, the second-order dispersion equation (3.12) and the leading order vertical structure function (3.16) are very good approximations.

By use of (4.3) it is easy to find that

$$\epsilon = -(n - \nu)\Delta \tag{4.5}$$

where Δ is a measure of nondimensional shear supercriticality:

$$\Delta \equiv \frac{\lambda - \lambda_c}{\lambda} \tag{4.5a}$$

and $\lambda_c = (2n\tilde{K} - \alpha)^{-1}$ is the critical shear for which $\eta = \eta_c$, and the neutral mode exists. Therefore, ϵ is a measure of the supercriticality.

If we substitute an asymptotic expansion of the form

$$\sigma = |\Delta|^{1/2}\sigma_1 + |\Delta|\sigma_2 + |\Delta|^{3/2}\ln|\Delta|^{1/2}\sigma_3 + |\Delta|^{3/2}\sigma_4 + \cdots$$

into the approximate dispersion equation (3.12), we obtain

$$\sigma = \Delta\left[\frac{1}{2}\left(1 - \frac{\nu}{2n}\right) \mp \Delta^{1/2}\frac{(\pi \pm \pi/2)}{2\sqrt{2n}} \pm \frac{i}{\sqrt{2n}}\left[1 + \Delta\ln\Delta^{1/2}\frac{(n-\nu)}{2} - \frac{\Delta}{4}\left(1 - \frac{\nu}{2n} + \ln 2n\right)\right]\right], \quad \text{for} \quad \Delta > 0;$$

$$\sigma = \pm\sqrt{\frac{|\Delta|}{2n}}\left[1 \mp \sqrt{\frac{n|\Delta|}{2}}\left(1 - \frac{\nu}{2n}\right) - \frac{\Delta}{2}\ln|\Delta|^{1/2}(n-\nu) + \frac{|\Delta|}{4}\left(1 - \frac{\nu}{2n} + \ln 2n\right)\right] \mp i|\Delta|^{3/2}\frac{\pi(3/2 \mp 1/2)}{2\sqrt{2n}}, \quad \text{for} \quad \Delta < 0. \tag{4.6}$$

Equation (4.6) shows that the growth rate is $O(\Delta^{1/2})$ for supercritical shear $\Delta > 0$ (strong instability) and $O(|\Delta|^{3/2})$ for subcritical shear, $\Delta < 0$ (weak instability) in accord with the results of Miles (1964).

5. The effects of the Newtonian cooling and Ekman dissipation

By use of the third-order dispersion equation we calculated the complex phase speed in the presence of Newtonian cooling. Corresponding calculations for the Ekman dissipation are described in Wang (1984); here we will content ourselves with a summary of his findings. Figure 7 displays the imaginary part of phase speed c_I as functions of total wavenumbers and Newtonian cooling coefficient μ. We see that the Newtonian cooling is much more effective in reducing c_I for the Green modes than for the Charney modes as expected, since, for a given μ, μ/k is much larger for the Green than for the Charney modes. Thus, the Newtonian cooling

TABLE 1. The wavelength, in 10^3 km, of the most unstable Charney mode (L_{MUCM}) as a function of vertical shear λ_* (10^{-3} s^{-1}), central latitude θ_0 (°N), and the rate of linear variation of stability parameter, $\hat{\alpha}$, for both Boussinesq and non-Boussinesq models. L_{MUCM} increases with increasing vertical shear and central latitude and decreases when the mass convergence effect, D/H, and the variation of the stability parameter with height, $\hat{\alpha}$, are included.

	Boussinesq fluid				Non-Boussinesq fluid							
	$\hat{\alpha}=0$ λ_* ($\times10^{-3}$ s^{-1})				$\hat{\alpha}=0$ λ_* ($\times10^{-3}$ s^{-1})				$\hat{\alpha}=0.16$ λ_* ($\times10^{-3}$ s^{-1})			
θ_0 (deg)	1.0	1.5	2.0	2.5	1.0	1.5	2.0	2.5	1.0	1.5	2.0	2.5
30	3.83	5.23	6.97	8.71	2.65	3.28	3.95	4.51	2.46	3.02	3.60	4.01
35	4.22	5.76	7.67	9.59	2.79	3.42	4.07	4.61	2.58	3.13	3.69	4.15
40	4.62	6.30	8.40	10.50	2.92	3.55	4.18	4.69	2.69	3.23	3.77	4.20
45	5.04	6.42	9.17	11.00	3.06	3.70	4.29	4.77	2.80	3.33	3.85	4.26
50	5.51	7.51	10.01	12.51	3.20	3.81	4.40	4.86	2.91	3.44	3.94	4.31

should be retained when studying the Green mode dynamics and could be omitted when studying the Charney mode dynamics. Although Newtonian cooling damps the fast growing modes, in the region very close to the inviscid critical points ($\eta_c = 2n$) a small amount of Newtonian cooling tends to produce an weak growth which essentially bridges the two adjacent unstable regions. In contrast to the weak destabilizing effect of the small Newtonian cooling on the neutral modes, Ekman dissipation never has such an effect as found previously by Card and Barcilon (1982). For both damping, the wavelength of the most unstable Green mode does not change with increasing damping; however, the wavelength of the most unstable Charney mode was reduced as the Newtonian cooling increases (see Fig. 7).

Figure 8 shows a pronounced increase in the eastward phase speed of the modes near the critical point $\eta_c = 2$ as the Newtonian cooling increases. The presence of μ raises slightly the eastward phase speed of the fast moving Charney mode, but reduces slightly the eastward phase speed of the fast moving Green mode. We also conclude that the Newtonian cooling will have an appreciable influence on the group velocity of these waves.

We consider the local behavior of the solution near the critical points η_c. In the presence of Newtonian cooling the quantity ϵ in (3.11) becomes [recall (3.3d) and (4.5)]

$$\epsilon = -(n-\nu)\Delta - i\mu\frac{S_0K^2}{2k\tilde{K}}. \tag{5.2}$$

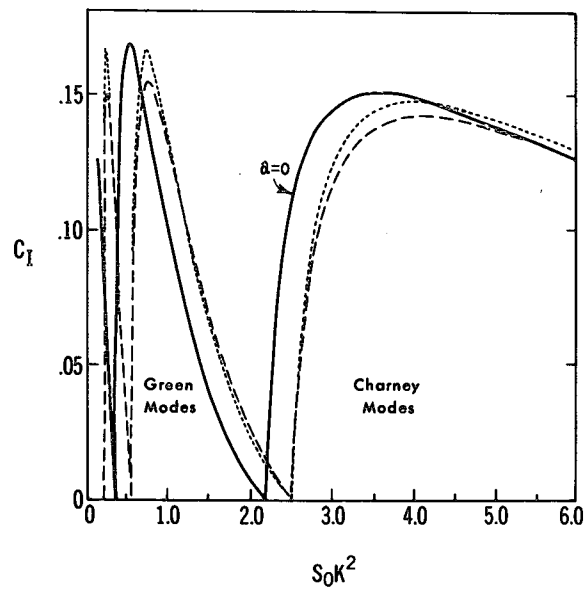

FIG. 5. Imaginary part of phase speed, c_I vs total wavenumber squared S_0K^2 when N^2 is constant with height, i.e., when $\hat{\alpha}=0$ (solid line), when the full dependence on $\hat{\alpha}$ is retained (dashed line), and when the approximation (4.3) is made (dotted line). The calculation was carried out for $J=10$, $\hat{\alpha}=0.1$, $\lambda_* = 1.2\times10^{-3}$ s^{-1}.

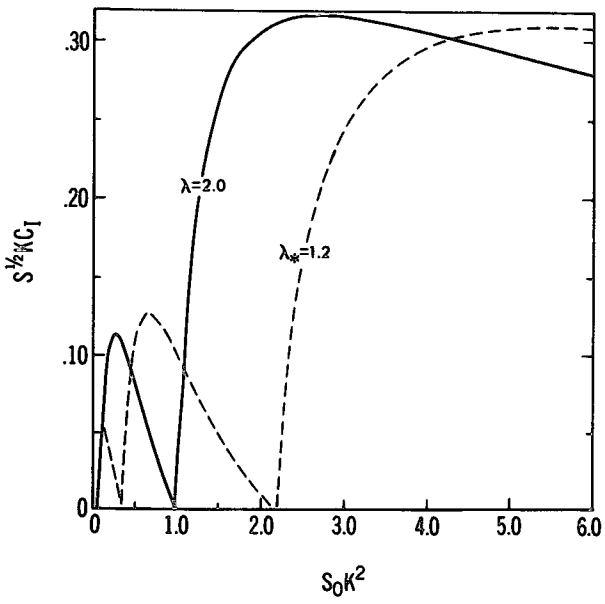

FIG. 6. Plot of growth rate $S_0^{1/2}Kc_I$ against the total wavenumber squared, S_0K^2, for two typical values of vertical shear: $\lambda_* = 2.0\times10^{-3}$ s^{-1} (solid line) and $\lambda_* = 1.2\times10^{-3}$ s^{-1} (dashed line), showing the sensitivity of the growth rate to changes in the vertical shear ($\hat{\alpha}=0$).

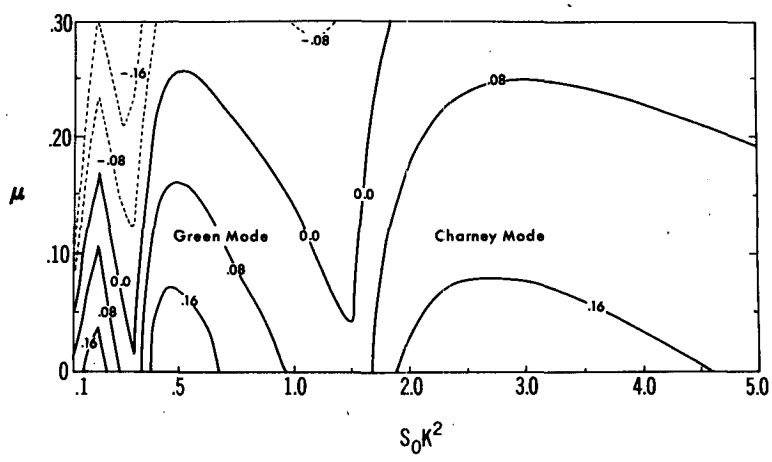

FIG. 7. Contour plot of the imaginary part of phase speed c_I as a function of total wavenumber and Newtonian cooling coefficient. The inviscid neutral wavenumbers are around $S_0K^2 = 0.3$ and 1.50 in the presence of the $\hat{\alpha}$-effect ($\hat{\alpha} = 0.16$); the small μ destabilizes the zonal flow and eliminates the existence of the neutral modes.

Assume that the eigenvalue, σ, as well as ϵ, δ are small, as can be verified *a posteriori,* then in the vicinity of the critical points, the second-order dispersion equation (3.12) can be simplified so as to become

$$\sigma^2(n-\nu) + \sigma\left[\left(1-\frac{\nu}{2n}\right)\epsilon + i\frac{\delta K^2}{k}\right] - \frac{\epsilon}{2n}\left(1 - i\delta\frac{K^2}{k}\right) = 0 \quad (5.3)$$

after we neglect the small terms of $O(\sigma^2\delta)$ and $O(\epsilon\sigma^2 \times \ln\sigma)$. The solution of the quadratic in σ found in (5.3) gives at once

$$c = -i\frac{\mu}{k} + \frac{1}{2\tilde{K}(n-\nu)}\left\{-\left(1-\frac{\nu}{2n}\right)\epsilon - i\delta\frac{K^2}{k} \pm \left[\left(1-\frac{\nu}{2n}\right)^2\epsilon^2 - \delta^2\frac{K^4}{k^2} + 2i\delta\frac{K^2}{k}\epsilon\left(1-\frac{\nu}{2n}\right) + \frac{2\epsilon}{n}(n-\nu)\left(1 - i\delta\frac{K^2}{k}\right)\right]^{1/2}\right\}. \quad (5.4)$$

Letting $\delta = \hat{\alpha} = 0$ in (5.4), we obtain

$$c_R = \mp\frac{|\Delta|^{1/2}}{2\tilde{K}\sqrt{n}}\left\{\left[1 + \left(\frac{\mu S_0K^2}{2\tilde{K}k\Delta(n-\nu)}\right)^2\right]^{1/2} - \frac{\Delta}{|\Delta|}\right\}^{1/2}, \quad (5.4a)$$

$$c_I = -\frac{\mu}{k} \pm \frac{|\Delta|^{1/2}}{2\tilde{K}\sqrt{n}}\left\{\left[1+\left(\frac{\mu S_0K^2}{2\tilde{K}k\Delta(n-\nu)}\right)^2\right]^{1/2} + \frac{\Delta}{|\Delta|}\right]\right\}^{1/2}; \quad (5.4b)$$

when $\mu = 0$, (5.4a, b) recover Miles (1964) results. Equation (5.4b) shows that the Newtonian cooling always gives rise to a damping term: $-\mu/k$, but may also destabilize the basic flow via the term found under the square root sign. When $1 \gg \mu^2 \gg \Delta^2$, i.e., in the regions very close to the critical points,

$$c_I = -\frac{\mu}{k} \pm \frac{1}{2\tilde{K}}\left[\frac{S_0K^2\mu}{2k\tilde{K}n(n-\nu)}\right]^{1/2} \sim O(\mu^{1/2}) \quad (5.5)$$

i.e., the order of c_I is determined by the second term. This weak instability is caused by the combined effect of small Newtonian cooling and very weak shear.

Let $\mu = \hat{\alpha} = 0$ in (5.3), and after neglecting terms of $O(\epsilon)$, it can be shown (Wang, 1984) that, when Ekman dissipation is present,

$$c = -\frac{i\delta K^2}{2k\tilde{K}(2-\nu)}\left[1 \pm \left(1 + \frac{2(n-\nu)^2k^2\Delta}{nK^4\delta^2}\right)\right]. \quad (5.6)$$

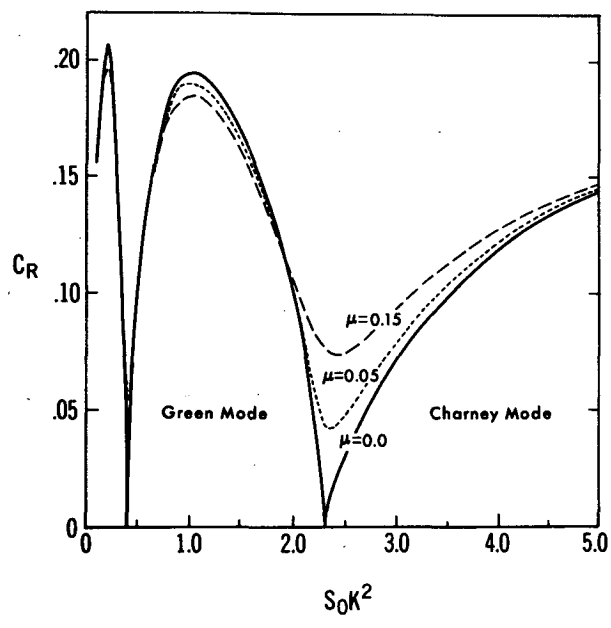

FIG. 8. Phase speed c_R as a function of total wavenumber for different Newtonian cooling $\mu = 0.15$, (dashed line), 0.05 (dotted line), 0.0 (solid line). Inviscid neutral wavenumber is around $S_0K^2 = 0.48$, 2.30, in the absence of $\hat{\alpha}$-effect.

When $\delta \gg O(\Delta^{1/2})$ and $\Delta \to 0$,

$$c = \begin{cases} -i\delta K^2/k\tilde{K}(2-\nu) \\ 0, \end{cases}$$

i.e., there is a damped mode of order δ and a neutral mode. This case is quite different from the one of small Newtonian cooling given by (5.5) in which the mode growing has a c_I of order of $\mu^{1/2}$ and the other is damped. Therefore, Ekman dissipation is never destabilizing while Newtonian cooling may be. This behavior can be contrasted with that of the Eady or the two-layer models (Holopainen, 1961; Williams and Robinson, 1974; Romea, 1976) having a single, lower Ekman layer, in which the Ekman dissipation destabilizes part or all of the wave band which was neutral in its absence.

6. Vertical structures

From (3.16b) we write the modulus of the stream-function for the Green modes as

$$|\tilde{\Phi}(z; 4+2\epsilon)| = \tilde{K}\left[(z-c_R)^2 + \left(c_I - \frac{\mu}{k}\right)^2\right]^{1/2} \times \left\{[1-\tilde{K}(z-c_R)]^2 + \tilde{K}^2\left(c_I - \frac{\mu}{k}\right)^2\right\}^{1/2} e^{pz+\tilde{K}c_R} \quad (6.1)$$

where $p \equiv (\alpha/2) - \tilde{K}$, and $|\tilde{\Phi}| \to 0$ as $z \to \infty$.

The structure of the unstable Green mode, calculated by use of the approximate formula (6.1), is shown in Fig. 11. Compared to the Charney mode (Fig. 9), the Green mode has more of an internal wave structure due to the higher location of its turning point. The extrema of $|\tilde{\Phi}|$ are the roots of the following quartic in z:

$$\tilde{K}^2 p z'^4 + 2\tilde{K}(\tilde{K}-p)z'^3 + \left\{p - 3\tilde{K} + 2\tilde{K}^2 p \times \left(c_I - \frac{\mu}{k}\right)^2\right\} z'^2 + z'\left[1 + 2\tilde{K}(\tilde{K}-p)\left(c_I - \frac{\mu}{k}\right)^2\right] + \left(c_I - \frac{\mu}{k}\right)^2\left[p - \tilde{K} + p\tilde{K}^2\left(c_I - \frac{\mu}{k}\right)^2\right] = 0,$$

where

$$z' \equiv z - c_R.$$

For strongly unstable Green modes, $(c_I - (\mu/k))^2 \ll 1$, one root is approximately given by $z_1 = c_R$; knowledge of that root reduces the degree of that quartic by one and the remaining roots are found to be

$$\left.\begin{aligned} z_2 &\approx c_R + \tilde{K}^{-1} \\ z_3 &\approx c_R + 0.5\tilde{K}^{-1} \\ z_4 &\approx c_R - \frac{2}{p} + \frac{1}{2\tilde{K}} \end{aligned}\right\}. \quad (6.2)$$

It can be shown that $|\tilde{\Phi}(z; 4+2\epsilon)|$ reaches maxima at z_3 and z_4 and minima at z_1, z_2, the absolute minimum being found at z_2 which is near the tropopause. For typical winter parameters the lower maximum is at mid-tropospheric levels while the upper maximum is found in the middle stratosphere for the most unstable Green mode. The ratio of the moduli at the two maxima is given by,

$$\frac{|\tilde{\Phi}(z_4; 4+2\epsilon)|}{|\tilde{\Phi}(z_3; 4+2\epsilon)|} = \frac{16\tilde{K}^2}{p^2 e^2} \sim 10,$$

where $e = 2.1718\cdots$.

Equations (6.1) and (6.2) also show that the wave amplitude depends upon α, $\tilde{K}$, c_R and c_I. Because $|c| \ll 1$, we anticipate that the amplitude is primarily controlled by α, $\tilde{K}$, especially above the tropopause. The dependence on α and $\tilde{K}$ is also found in the exponential [see (6.1)]: Small changes in α and K, like those due to the presence of $\hat{\alpha} \neq 0$, will have a profound effect on the vertical structure of the modulus, $|\tilde{\Phi}|$; in the case of the Green modes, $\tilde{K}$ and p are much smaller than their corresponding values in the Charney modes and the effects of $\hat{\alpha}$ are more pronounced.

Table 2 shows the role of the linear increase of the static stability on the Green mode dynamics. In the calculation we take the central latitude at 40°, the width of the westerlies is 5000 km, the density scale height is 8 km, the vertical shear is 1.2 m s^{-1} km. We considered two cases:

1) $N^2 = \bar{N}^2 = 2.30 \times 10^{-4}$ s^{-2}
2) $N^2 = N_0^2(1 + \hat{\alpha}z)$, where $N_0^2 = 2.0 \times 10^{-4}$ s^{-2}, $\hat{\alpha} = 0.1$.

Below the stratopause (~6 density scale heights), the vertical averaged Brunt-Väisälä frequencies are about the same in the two cases, to facilitate comparison. The results, shown in Table 2, demonstrate that the increase of N^2 with height favors the selection of a shorter wave as the most unstable Green mode. Also, the height of the maximum wave amplitude is considerably increased.

While, α, $\tilde{K}$ control the amplitude of $|\tilde{\Phi}|$ for larger values of z, the complex phase speed has a non-negligible influence on the wave structure in the troposphere, especially near the ground, as can be seen from (6.1).

TABLE 2. Effects of the increasing static stability on the Green mode.

	$N^2 = \bar{N}^2$	$N^2 = N_0^2 \times (1 + 0.1z)$
Wavelength of the most unstable Green mode (km)	11400	9900
Heights of the maximum amplitude of the stream-function modulus (km) for		
1) most unstable Green mode ($\eta = 3.4$)	27	34
2) strongly unstable Green mode ($\eta = 3.8$)	32	41

Thus, Ekman damping and Newtonian cooling will be felt more dramatically in the lower structure of the modulus, $|\tilde{\Phi}|$.

The phase of $|\tilde{\Phi}|$ for the strongly unstable Green modes can be found from (6.1) and can be expressed as

$$ph\tilde{\Phi}(z;\,4+2\epsilon)=\tilde{\theta}+\arctan\left[\frac{\cos\tilde{K}c_I'(2\tilde{K}z'-1)+\sin\tilde{K}c_I'[z'(1-\tilde{K}z')+\tilde{K}c_I'^2]}{\cos\tilde{K}c_I'[z'(1-\tilde{K}z')+\tilde{K}c_I'^2]-\sin\tilde{K}c_I'(2\tilde{K}z'-1)c_I'}\right] \tag{6.3}$$

where $z'\equiv z-c_R$, $c_I'\equiv c_I-\mu/k$, and

$$\tilde{\theta}=\begin{cases}0, & \text{when the denominator} > 0\\ \pi, & \text{when the denominator} < 0\\ & \text{and the numerator} > 0\\ -\pi, & \text{when the denominator} < 0\\ & \text{and the numerator} < 0.\end{cases}$$

For eastward moving and amplifying waves $ph\tilde{\Phi}\sim\arctan(c_I'/c_R)-\pi$ near the ground (as in the Charney case) while $ph\tilde{\Phi}\sim\arctan(\sin\tilde{K}c_I')+\pi$ as $z\to\infty$, which is larger than the Charney mode phase change by nearly π (also see Figs. 10 and 12). As seen from Fig. 12, most of the phase change of the Green mode occurs in the troposphere and lower stratosphere since, for $z\geq 2$, the phase remains nearly constant indicating that these modes have a barotropic structure in the stratosphere. Equation (6.3) reveals that the complex phase speed controls the structure of these phase changes with height; the same statement is valid for the Charney mode.

For completeness, Fig. 9, 10, 11, 12 show the moduli and phases of temperature and vertical velocity perturbations.

7. Energetics of the Charney and Green Modes

When the basic state current U varies only with height, the only source of energy for the growing disturbances is the zonal available potential energy. The conversion of that energy $\bar{E}_p$ to eddy available potential energy E_p is effected by the northward heat flux, i.e.,

$$\langle\bar{E}_p\cdot E_p\rangle=\int_{-1}^{1}dy\int_0^\infty\frac{\rho_s}{S}\overline{\frac{\partial\phi}{\partial x}\frac{\partial\phi}{\partial z}}\,dz$$

$$=\int_0^\infty\frac{\rho_s}{S}\,\mathrm{HHF}(z)dz \tag{7.1}$$

where the overbar denotes an x-average, and $\rho_s=\rho_0e^{-z}$. The poleward heat flux per unit mass at a given z-level, HHF(z), is defined as

$$\mathrm{HHF}(z)=\int_{-1}^{1}\overline{\frac{\partial\phi}{\partial x}\frac{\partial\phi}{\partial z}}\,dy$$

$$=ik\left(\tilde{\Phi}\frac{\partial\tilde{\Phi}_*}{\partial z}-\tilde{\Phi}_*\frac{\partial\tilde{\Phi}}{\partial z}\right)e^{2kc_It}\sim|\tilde{\Phi}|^2\frac{\partial}{\partial z}(ph\tilde{\Phi}). \tag{7.2}$$

When the phase increases with height, $\partial(ph\tilde{\Phi})/\partial z>0$ and the horizontal heat flux is poleward. The generation of eddy kinetic energy in our model is only due to the conversion of eddy available potential energy E_p to eddy kinetic energy E_k, since a meridional shear in the basic state is absent. This conversion can be represented in terms of the vertical heat flux per unit mass at a given z-level as

$$\mathrm{VHF}(z)=\int_{-1}^{1}dy\,\overline{\frac{\partial\phi}{\partial z}\left[\frac{\partial\phi}{\partial x}-\left(\frac{\partial}{\partial t}+z\frac{\partial}{\partial x}\right)\frac{\partial\phi}{\partial z}-\mu\frac{\partial\phi}{\partial z}\right]}$$

$$\sim|\tilde{\Phi}|^2\frac{\partial}{\partial z}(ph\tilde{\Phi})$$

$$-\left(c_I+\frac{\mu}{k}\right)\left[\left(\frac{\partial}{\partial z}|\tilde{\Phi}|\right)^2+|\tilde{\Phi}|^2\left(\frac{\partial}{\partial z}ph\tilde{\Phi}\right)^2\right] \tag{7.3}$$

so that

$$\langle E_p\cdot E_k\rangle=\int_0^\infty\frac{\rho_s}{S}\,\mathrm{VHF}(z)dz. \tag{7.4}$$

The first term on the right-hand side in (7.3) represents the HHF and the second term is simply the product of $(c_I+\mu k^{-1})$ times the eddy available potential energy.

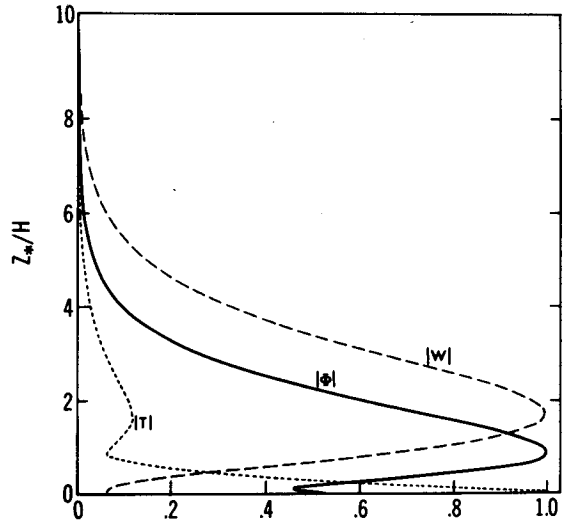

FIG. 9. The moduli of geopotential stream function (solid line), temperature (dotted line), and vertical velocity (dashed line) as functions of height for strongly unstable Charney modes in the presence of Newtonian cooling and Ekman dissipation calculated by use of the lowest order solution. ($\eta=1.8$, $\lambda_*=1.2\times10^{-3}$ s^{-1}, wave 7 around 40°N).

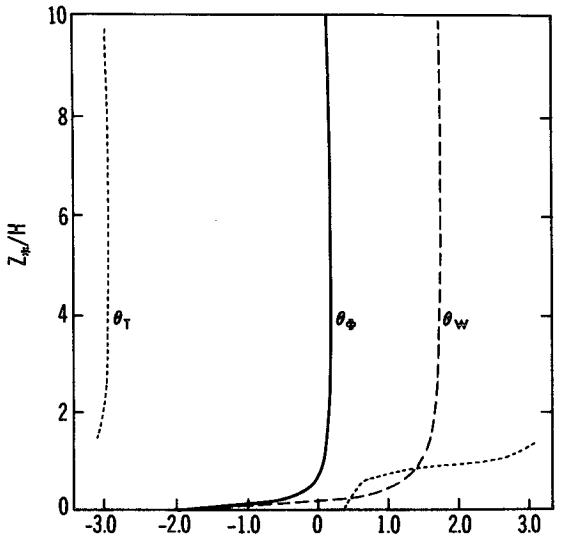

FIG. 10. As in Fig. 9 except for the phases θ_Φ, θ_T, θ_w.

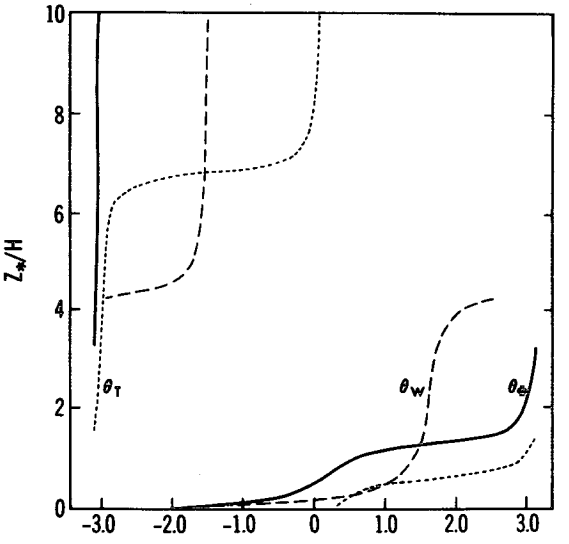

FIG. 12. As in Fig. 11 except for the phases θ_Φ, θ_T, θ_w.

Figure 13 shows that, for the strongly unstable Charney modes, the poleward heat flux per unit mass is large in the lower tropospheric layers with a maximum at the ground since both the streamfunction modulus and the slope of the phase tilt reach their maximum at the ground. However, as can be seen from Fig. 14, the poleward heat transport for the strongly unstable Green modes exhibits a significant peak in the middle stratosphere in accord with similar findings by other investigators (Kuo, 1979; Fullmer, 1982; Branscome, 1983). This important feature implies that planetary waves may play an important part in changing the mean temperature distribution in the stratosphere. It also implies that the energy sources for the growing Green modes come from both the troposphere (near the ground) and the stratosphere. Nevertheless, the dependence of the stability properties of the Green modes on the lower boundary is much weaker than for the Charney modes since the latter extract their eddy energy exclusively from layers close to the boundary.

Figures 13 and 14 also show the vertical distribution of vertical heat flux per unit mass, VHF(z), for the

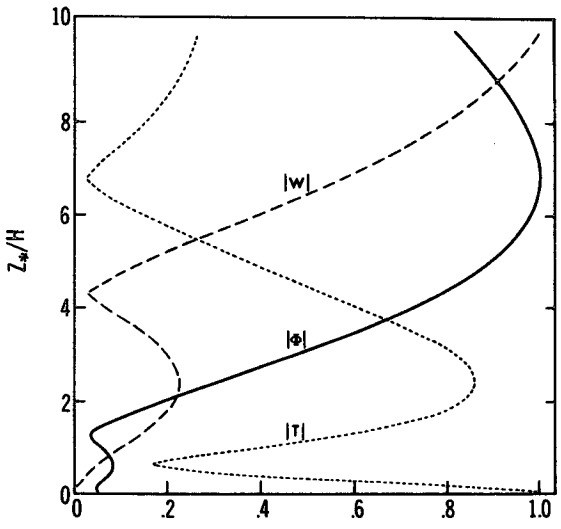

FIG. 11. The moduli of geopotential streamfunction (solid line), temperature, (dotted), and vertical velocity (dashed line) as functions of height for strongly unstable Green modes in the presence of Newtonian cooling and Ekman dissipation calculated by use of the lowest order solution. ($\eta = 3.8$, $\lambda_* = 1.3 \times 10^{-3}\ s^{-1}$, $\hat{\alpha} = 0.1$, wave 2).

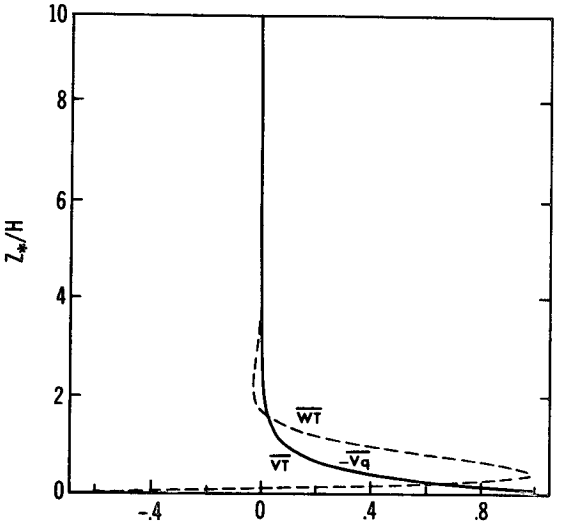

FIG. 13. Variations of the poleward heat flux $\overline{vT}$ (dotted line), vertical heat flux $\overline{wT}$ (dashed line), and equatorward potential vorticity flux $-\overline{vq}$ (solid line) per unit mass, with height for strongly unstable Charney modes calculated by use of the lowest order solution. The dotted line coincides with solid line.

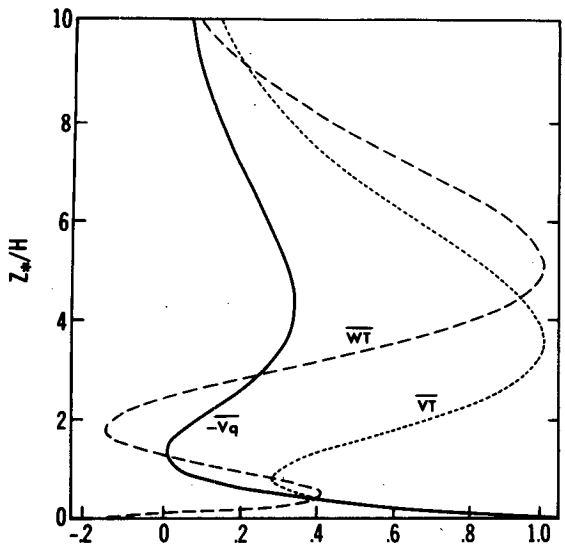

FIG. 14. As in Fig. 13, except for strongly unstable Green modes (parameters are the same as Fig. 11).

Charney and Green modes. This flux must vanish near the ground in the absence of Ekman dissipation, but since we used the lowest approximation for the complex streamfunction modulus this flux is negative near $z = 0$. The peak for the Charney modes is in the lower troposphere ($z \sim 3$ km) while the Green modes have a double peak, the major one being in the upper stratosphere and the minor one in the middle troposphere. Another noticeable difference is that, just above the tropopause, the fluxes of the Green modes are much larger than the fluxes of the Charney modes, both being negative. Therefore, the kinetic energy of the Charney modes is generated mainly in the lower and middle troposphere while the kinetic energy of the Green modes is generated in the middle troposphere and middle stratosphere with significant destruction near the tropopause.

In the presence of a local energy source provided by vertical shear of the mean zonal flow, the necessary condition for the existence of *untrapped* waves in a region was given by Holton (1974). In terms of our model notation that condition is

$$S_0 K^2 \leqslant b \frac{(z - c_R)}{|c - z|^2}. \tag{7.5}$$

For typical winter parameters, and for wave 2, the above criterion gives, approximately, $z \leqslant 5.5$. Above 5–6 scale heights, the vertical flux of the unstable Green modes will decrease exponentially.

Finally, the equatorward transport of eddy potential vorticity is an important quantity to consider because $-\rho_s \overline{vq}$ measures the interaction between the mean flow and the wave field (Lindzen *et al.*, 1980). For both the Charney and Green modes the maxima are found near $z = 0$ (see Figs. 13 and 14) which corresponds to the top of the Ekman layer. The numerical calculation given by Pfeffer (1981) (his Fig. A3) shows that the winter average distribution of $-\overline{vq}$ due to heat flux contribution and due to transient waves has a major maximum around 850 mb at 30–40°N and a minor maximum around 400 mb at 50–60°N. Although the horizontal and the vertical heat fluxes of the Green modes have their main peaks in the stratosphere, the potential vorticity flux of these modes, $-\overline{vq}$, is primarily restricted to the lower troposphere with a minor peak in the stratosphere. This agrees with the conclusion of Lindzen *et al.* (1980), although their analysis, based on the ideas of overreflection of vertically propagating generalized Rossby waves, was primarily made for the Charney modes.

8. Conclusions and discussions

The present study extends the Charney model for baroclinic instability by including Newtonian cooling, Ekman layer dissipation and a linear vertical variation of the basic stability parameter. The dispersion equation and the vertical structure of the strongly unstable modes can be well approximated by a second-order transcendental equation and a generalized Laguerre polynomial multiplied by an exponential function, respectively. These approximate solutions provide us with a useful tool for the stability analysis and with more intuitive physical understanding of the factors controlling the instability.

For typical midlatitude atmospheric winter parameters the slowly eastward propagating planetary wave 2, 3, and 4 may be viewed as the atmospheric counterparts of the most unstable Green mode. It is shown that the wavelength ratio of the most unstable Green mode to most unstable Charney mode, which is about 2.5 to 3 for typical midlatitude winter conditions, is only weakly dependent upon the properties of the basic flow: vertical shear, stratification, β-effect, Coriolis parameter etc. The growth rate ratio of the most unstable Green mode to the most unstable Charney mode is the inverse of the corresponding wavelength ratio. However, the wavelengths of both most unstable modes may experience significant changes caused by the changes of the basic state. Stronger vertical shear, faster rotation rate, and weaker β-effect favor the selection of longer waves.

Above the midtroposphere, the amplitude of the strongly unstable waves is mainly controlled by the total wavenumber and the increasing static stability parameter, while the supercritical shear, Newtonian cooling and Ekman dissipation control the amplitude near the ground and the phase changes with height via their effect on the complex phase speed. Contrasted with the trapped Charney modes in the troposphere, the Green modes have their main peaks in the stratosphere and these are an order of magnitude larger than the minor peaks found in the midtroposphere. The

total phase change with height for the Green mode is larger than that of Charney mode by 180°. The tilt of the constant phase line of the Green modes occurs from the ground up to the tropopause, but in the stratosphere the Green mode features a barotropic structure.

Calculations show that poleward and vertical heat fluxes due to the unstable Green modes display a double peak feature. This feature, which is wavenumber dependent, has its main peak in the stratosphere. The available potential energy for the growing Green modes comes from both the troposphere (near the lower boundary) and the stratosphere. The kinetic energy of the Green modes is generated in the middle troposphere and middle stratosphere with significant destruction near the tropopause. Although the dependence of the stability properties of the Green modes on the lower boundary is much weaker than for the Charney modes, the interaction between the mean flow and the Green modes is primarily confined to the lower troposphere.

The Newtonian cooling (Ekman dissipation) is an effective energy sink for Green mode (Charney mode). Nevertheless, in the immediate vicinity of the inviscid neutral wavelength, small amounts of Newtonian cooling combined with super- or subcritical shear have a weak destabilizing effect and this weak instability serves as a bridge between adjacent unstable regimes. On the contrary, small Ekman dissipation produces a damped wave band between these unstable regimes.

The present model assumes a linear increase of N^2 with height. This representation misses the sharp change of N^2 near tropopause and stratopause, but still gives the general trend of the vertical variation of the N^2 below the stratopause. Because of the exponential decay of the density and of the wave fields above the turning points, the unrealistic infinite increase of both U and N^2 are not expected to influence the present results appreciably. The vertical increase of the static stability was found to have an appreciable influence on the Green mode dynamics: it reduces the wavelength of the most unstable modes, considerably affects the growth rate for a given wavenumber, and significantly raises the level of maximum wave amplitude.

The above features of the Green modes, though inferred from an idealized analytical model, agree in many respects with numerical model results and with observed transient planetary waves. Their growth rate is smaller but significant compared to that of the cyclone scale waves. Their available potential and kinetic energy may be generated at much higher altitude. The exponential decrease of the vertical flux of energy for the unstable Green modes occurs only after several scale heights; the dissipative time scale for the Green modes is longer than that of the Charney modes. Since they extended to higher altitude, their growth is not suppressed by the wave mean flow interaction as quickly as is that of the Charney modes that are restricted to the lower troposphere. Therefore, the Green modes, by having a longer life time, will play an important role in the variation of the general circulation of the atmosphere on the longer time scales.

Acknowledgments. We gratefully acknowledge partial support of the Office of Naval Research, under Grants N00014-78-C-0106, N00014-77-C-0265 (B.W. and A.B.) and N00014-75-C-0877 NR062-547 (L.N.H.) and National Science Foundation Grant ATM 8418624 (B.W. and A.B.).

APPENDIX A

Evaluation of $\mathcal{C}_1(\eta)$ and $\mathcal{C}_2(\eta)$

Consider the system given by (3.2), i.e.,

$$\xi \frac{d^2\Phi}{d\xi^2} + (\eta - \xi)\Phi = 0, \tag{A1}$$

$$e^{\nu\xi}\Phi \to 0, \quad \text{as} \quad \xi \to \infty, \tag{A2}$$

and

$$\sigma\left(\frac{d\Phi}{d\xi} + \nu\Phi\right) + \left(1 - i\delta\frac{K^2}{k}\right)\Phi = 0 \tag{A3}$$

at $\xi = -\sigma$. A solution of (A1) can be written as

$$\Phi(\xi; \eta) = \mathcal{C}_1(\eta)\Phi_1(\xi; \eta) + \mathcal{C}_2(\eta)\Phi_2(\xi; \eta), \tag{A4}$$

where $\Phi_{1,2}$ are the complementary solutions obtained by means of the Frobenius method applied at $\xi = 0$; these are:

$$\Phi_1(\xi; \eta) = \sum_{j=1}^{\infty} a_j\xi^j,$$

$$\Phi_2(\xi; \eta) = \Phi_1(\xi; \eta)\ln\xi + \sum_{j=0}^{\infty} b_j\xi^j, \tag{A5}$$

where

$$a_1 = 1, \quad a_2 = -\eta/2,$$

$$a_j = (a_{j-2} - \eta a_{j-1})/[j(j-1)], \quad j \geq 3$$

and

$$b_0 = -1/\eta, \quad b_1 = 0$$

$$b_j = [b_{j-2} - \eta b_{j-1} - (2j-1)a_j]/[j(j-1)], \quad j \geq 2.$$

Any solution of (A1) has the form (A4); we shall now determine particular $\mathcal{C}_1$ and $\mathcal{C}_2$ so that (A2) is satisfied; any solution of (A1) and (A2) will then be a multiple of this one. Once Φ is known it is a simple matter to substitute it in (A3) and determine the dispersion relation for the eigenvalue σ, or for the complex phase speed c.

Since Equation (A1) has coefficients linear in ξ, Laplace integral representation of the solution may be found. Let

$$\Phi(\xi) = \frac{1}{2\pi i}\oint_{\mathcal{L}} e^{p\xi}\mathcal{F}(p)dp \tag{A6}$$

where the contour $\mathcal{L}$ in the complex p-plane and the function $\mathcal{F}(p)$ remain to be determined so that (A1)

and (A2) are satisfied. Using (A6) in (A1) we find that, after some simple manipulations, (A1) is satisfied if

$$\oint_{\mathcal{L}} e^{p\xi}(p^2-1)\left[\frac{d\mathcal{F}}{dp}+\frac{(2p-\eta)}{(p^2-1)}\mathcal{F}\right]dp - (p^2-1)\mathcal{F}e^{p\xi}|_{\mathcal{L}}=0.$$

Requiring that the integrand and the integrated term vanish, we obtain

$$\mathcal{F}(p)=\text{constant}\cdot(p^2-1)^{-1}\left(\frac{p-1}{p+1}\right)^{\eta/2} \tag{A7}$$

and

$$\left(\frac{p-1}{p+1}\right)^{\eta/2}\cdot e^{p\xi}|_{\mathcal{L}}=0. \tag{A8}$$

This last constraint is satisfied if $\mathrm{Re}\xi>0$ and if the contour approaches $-\infty$ along the Rep axis. In general, η need not be an integer and therefore to make (A7) unambiguous we must introduce a branch cut. Choose such a cut from $p=-1$ to $p\to-\infty$ and from $p=1$ to $p\to+\infty$ so (see Fig. A1) that

$$\left(\frac{p-1}{p+1}\right)^{\eta/2}=\left|\frac{p-1}{p+1}\right|^{\eta/2}e^{i(\eta/2)(\theta_1-\theta_2)}, \tag{A9}$$

where $0\leqslant\theta_1<2\pi$ and $-\pi\leqslant\theta_2<\pi$. Then,

$$\Phi(\xi)=\frac{1}{2\pi i}\oint_{\mathcal{L}}e^{p\xi}\left(\frac{p-1}{p+1}\right)^{\eta/2}\frac{dp}{p^2-1}, \tag{A10}$$

and since, from (A2), $\Phi e^{\nu\xi}\to 0$ as ξ approaches ∞ we demand that

$$\mathrm{Re}(p+\nu)<0 \tag{A11}$$

everywhere on the contour $\mathcal{L}$; this can be done since $\nu<1$.

We determine $\mathcal{C}_2(\eta)$ by evaluating (A10) at the regular singular point $\xi=0$ where $\Phi_1(0,\eta)=0$, $\Phi_2(0,\eta)=b_0=-1/\eta$. We find at once that

$$\mathcal{C}_2(\eta)=-\frac{\eta}{2\pi i}\oint_{\mathcal{L}}\left(\frac{p-1}{p+1}\right)^{\eta/2}\frac{dp}{p^2-1}. \tag{A12}$$

Evaluation of that integral is made easier if we define

$$p=\frac{1+w}{1-w}$$

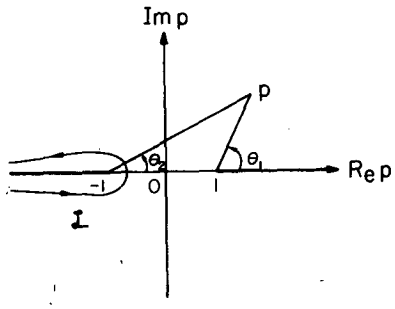

FIG. A1. Integration contour $\mathcal{L}$ in the p-plane.

and evaluate (A12) in the complex w-plane. We find

$$\mathcal{C}_2(\eta)=\frac{1}{2\pi i}(e^{i\pi\eta}-1), \tag{A13}$$

which vanishes, as it should, when $\eta=2n$ where n is a positive integer. These values of η correspond to the neutral modes of the Charney problem.

In order to determine $\mathcal{C}_1(\eta)$, form $\lim_{\xi\to0}\Phi'(\xi;\eta)$ where a prime stands for a ξ-derivative and from (A4) we find

$$\mathcal{C}_1(\eta)+\mathcal{C}_2(\eta)=\lim_{\xi\to0}[-\Phi'(\xi;\eta)+\mathcal{C}_2(\eta)\ln\xi]$$

or

$$\mathcal{C}_1(\eta)+\mathcal{C}_2(\eta)$$

$$=\lim_{\xi\to0}\left[-\mathcal{C}_2\ln\xi+\frac{1}{2\pi i}\int_{\mathcal{L}}e^{p\xi}p\left(\frac{p-1}{p+1}\right)^{\eta/2}\frac{dp}{p^2-1}\right]$$

$$=\lim_{\xi\to0}\left[-\mathcal{C}_2\ln\xi+\frac{1}{2\pi i}\int_{\mathcal{L}'}e^{\xi(1+w/1-w)}\times\frac{1+w}{1-w}w^{\eta/2}\frac{dw}{2w}\right],$$

where the path of integration $\mathcal{L}'$ is chosen as shown in Fig. A2. Notice that the requirement (A11) places a constraint on R, namely

$$R>\frac{1+\nu}{1-\nu}>3. \tag{A14}$$

After some manipulations the above equation becomes

$$\mathcal{C}_1(\eta)+\mathcal{C}_2(\eta)$$

$$=\lim_{\xi\to0}\left[-\mathcal{C}_2\ln\xi+\frac{1}{2\pi i}\int_{\substack{2\pi\\ w=Re^{i\theta}}}^{0}e^{2\xi/1-w}w^{\eta/2}\frac{dw}{1-w}+\mathcal{C}_2\int_1^R e^{2\xi/1-x}\frac{x^{\eta/2}dx}{1-x}\right]. \tag{A15}$$

The second term on the right hand side of (A15) is

$$\frac{1}{2\pi i}\int_{\substack{2\pi\\ (w=Re^{i\theta})}}^{0}w^{\eta/2}\frac{dw}{1-w}=\frac{1}{2\pi i}\int_{\substack{0\\ (w=Re^{i\theta})}}^{2\pi}\frac{w^{\eta/2}}{w}\times\left(1+\frac{1}{w}+\cdots\right)dw=\mathcal{C}_2R^{\eta/2}\sum_{n=0}^{\infty}\frac{R^{-n}}{\eta/2-n}. \tag{A16}$$

The third term on the right hand side of (A15) can be split to

$$\mathcal{C}_2\int_1^R e^{2\xi/1-x}\left(\frac{x^{\eta/2}-1}{1-x}+\frac{1}{1-x}\right)dx$$

$$=\mathcal{C}_2\int_1^R\frac{x^{\eta/2}-1}{1-x}dx+\mathcal{C}_2\int_1^R e^{2\xi/1-x}\frac{dx}{1-x}, \tag{A17}$$

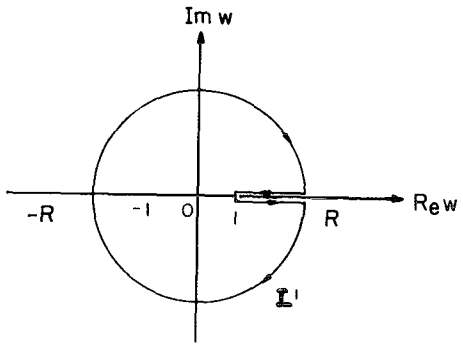

FIG. A2. Integration contour $\mathcal{L}'$ in the w-plane.

where

$$\int_1^R \frac{x^{\eta/2}-1}{1-x}\,dx = \ln R - R^{\eta/2}\sum_{n=0}^{\infty}\frac{R^{-n}}{(\eta/2-n)} - \sum_{n=1}^{\infty}\frac{R^{-n}}{n} + \frac{2}{\eta} - \frac{\eta}{2}\sum_{n=1}^{\infty}\frac{1}{n(n-\eta/2)}, \quad \text{(A18)}$$

and

$$\mathcal{C}_2\int_1^R e^{2\xi/1-x}\frac{dx}{1-x} = \mathcal{C}_2\int_{\infty}^{2\xi/R-1} e^{-v}\frac{dv}{v} = \mathcal{C}_2\gamma + \mathcal{C}_2\ln\xi + \mathcal{C}_2[\ln 2 - \ln(R-1)], \quad \text{(A19)}$$

where $\gamma = 0.57721566\cdots$ is Euler's constant. Now substituting (A16), (A17), (A18), and (A19) into (A15), and noticing

$$\ln(R-1) = \ln R - \sum_{n=1}^{\infty} R^{-n}/n,$$

and

$$-\frac{\eta}{2}\sum_{n=1}^{\infty}\frac{1}{n(n-\eta/2)} = \psi(1-\eta/2) + \gamma,$$

we finally obtain

$$\mathcal{C}_1(\eta) = \mathcal{C}_2(\eta)\cdot\left[-1 + \ln 2 + 2\gamma + \frac{1}{\eta} + \psi(1-\eta/2)\right] \quad \text{(A20)}$$

where $\psi(z)$ is the logarithmic derivative of the gamma function.

APPENDIX B

List of Symbols

A_j	Coefficients of the dispersion equation
A_z	eddy kinematic viscosity coefficient
B_j	coefficients of the dispersion equation
b	meridional gradient of the basic state potential vorticity multiplied by S.
$\mathcal{C}_1, \mathcal{C}_2$	coefficients of two linearly independent solutions of (3.2a)
c, c_R, c_I	complex phase speed of the normal modes, real and imaginary parts of c
C_P	specific heat at constant pressure
D	vertical length scale
$D_e \equiv (2A_z/f_0)^{1/2}$	a measure of Ekman layer depth
$\bar{E}_p$	zonal available potential energy
E_p, E_k	eddy available potential and kinetic energies
f_0	Coriolis parameter at latitude θ_0.
$H = RT_0/g$	density scale height
HHF	horizontal heat flux
k	nondimensional x-wavenumber
$K = (k^2 + l^2)^{1/2}$	nondimensional total wavenumber
$\tilde{K}$	modified total wavenumber defined by (3.3b)
L	horizontal length scale
L_D	Rossby radius of deformation
$L_\beta = R_a \cot\theta_0$	characteristic length scale for Burger motion
L_{MUCM}	wavelength of the most unstable Charney mode
L_{MUGM}	wavelength of the most unstable Green mode
l	nondimensional y-wavenumber
N, N_0	Brunt-Väisälä frequency and its value at the ground
p	pressure, also decaying exponent of structure function defined by (3.15)
$\dot{Q}$	diabatic heating rate per unit mass
R	gas constant
R_a	radius of the Earth
R_0	Rossby number
S, S_0	Stratification number and its value at $z = 0$
$V = \lambda_* D$	horizontal velocity scale
VHF	vertical heat flux
$\hat{\alpha} = (d/dz)N^2/N_0^2$	vertical derivative of N^2/N_0^2
$\alpha = \hat{\alpha} + D/H$	combination of non-Boussinesq and $\hat{\alpha}$-effects
β_0	meridional gradient of Coriolis parameter at latitude θ_0
$\gamma = 0.57721\cdots$	Euler's constant
δ	a measure of Ekman layer dissipation
$\Delta = (\lambda - \lambda_c)\lambda^{-1}$	a measure of shear supercriticality
ϵ	a measure of the deviation of the parameter η from its critical value η_c
$\eta = \tilde{b}/\tilde{K}$	generalized meridional gradient of basic state potential vorticity

	divided by modified total wavenumber
$\eta_c = 2n$	the critical value of η corresponding to neutral modes
η_M	the value of η corresponding to the most unstable modes.
θ_0	central latitude of f-plane
λ_*	vertical shear of basic zonal flow
λ	nondimensional shear defined by (2.10c)
$\lambda_c = (\tilde{K}\eta_c - \alpha)^{-1}$	nondimensional inviscid critical shear corresponding to neutral modes
$\mu = L/V\tau_*$	nondimensional Newtonian cooling coefficient
$\nu = \alpha/2\tilde{K}$	a quantity representing non-Boussinesq and $\hat{\alpha}$-effects
$\xi = \tilde{K}z - \sigma$	a transformed independent variable related to z.
$\rho_s = \rho_0 e^{-zD/H}$	density of the basic state
$\sigma = \tilde{K}\left(c + i\frac{\mu}{k}\right)$	eigenvalue of the model in terms of the complex phase speed c
τ_*	Newtonian cooling time
ϕ	perturbation stream function
Φ_1, Φ_2	two linearly independent solutions of the eigen equation
Φ	eigenfunction of the model
$\tilde{\Phi} = e^{\alpha z/2}\Phi$	vertical structure function of the normal modes
ψ	total streamfunction; also logarithmic derivative of the Gamma function
Ω	Earth's rotating rate.

REFERENCES

Branscome, L. E., 1983: The Charney baroclinic stability problem: approximate solutions and model structures. *J. Atmos. Sci.*, **40,** 1393–1409.

Burger, A. P., 1958: Scale consideration of planetary motions of the atmosphere. *Tellus,* **10,** 195–205.

Card, P. A., and A. Barcilon, 1982: The Charney stability problem with a lower Ekman layer. *J. Atmos. Sci.*, **39,** 2128–2137.

Charney, J. G., 1947: The dynamics of long waves in a baroclinic westerly current. *J. Meteor.*, **2,** 136–163.

——, and G. R. Flierl, 1981: Oceanic analogues of large-scale atmospheric motion, *Evolution of Physical Oceanography,* B. A. Warren and C. Wunsch, Eds., The MIT Press, 504–548.

Eady, E. T., 1949: Long waves and cyclone waves. *Tellus,* **1,** 33–52.

Fullmer, J., 1982: The baroclinic instability of highly structured one-dimensional basic states. *J. Atmos. Sci.*, **39,** 2371–2387.

Gent, P. R., 1974: Baroclinic instability of a slowly varying zonal flow. *J. Atmos. Sci.*, **39,** 2371–2387.

Geisler, J. E., and R. R. Garcia, 1977: Baroclinic instability at long wavelengths on a β-plane. *J. Atmos. Sci.*, **34,** 311–321.

Green, J. S. A., 1960: A problem of baroclinic stability. *Quart. J. Roy. Meteor. Soc.*, **86,** 237–251.

Grotjahn, R., 1980: Linearized tropopause dynamics and cyclone development. *J. Atmos. Sci.*, **37,** 2396–2406.

Hartmann, D. L., 1976: The structure of the stratosphere in the Southern hemisphere during late winter 1973 as observed by satellite. *J. Atmos. Sci.*, **33,** 1141–1154.

——, 1979: Baroclinic instability of realistic zonal-mean states to planetary waves. *J. Atmos. Sci.*, **36,** 2336–2349.

Held, I. M., 1978: The vertical scale of an unstable baroclinic wave and its importance for eddy heat flux parameterization. *J. Atmos. Sci.*, **35,** 572–576.

Holton, J. R., 1974: On the trapping of unstable baroclinic waves. *J. Atmos. Sci.*, **31,** 220–2222.

——, 1975: *The Dynamic Meteorology of the Stratosphere and Mesosphere, Meteor. Monogr.*, No. 47, Amer. Meteor. Soc.

Holopainen, E. O., 1961: On the effect of friction in baroclinic westerly current. *Tellus,* **13,** 363–367.

Kuo, H. L., 1979: Baroclinic instabilities of linear and jet profiles in the atmosphere. *J. Atmos. Sci.*, **36,** 2360–2378.

Leovy, C. B., and Webster, 1976: Stratospheric long waves: Comparison of thermal structure in the Northern and Southern Hemisphere. *J. Atmos. Sci.*, **33,** 1524–1638.

Lindzen, R. S., and A. J. Rosenthal, 1981: A WKB asymptotic analysis of baroclinic instability. *J. Atmos. Sci.*, **38,** 619–629.

——, Farrell, B. and Tung, K. K., 1980: The concept of wave overreflection and its application to baroclinic instability. *J. Atmos. Sci.*, **37,** 44–63.

Mechoso, C. R., and Hartmann, D. L., 1982: An observational study of traveling planetary waves in the Southern Hemisphere. *J. Atmos. Sci.*, **39,** 1921–1934.

Miles, J. W., 1964: A note on Charney's model of zonal-wind instability. *J. Atmos. Sci.*, **21,** 451–452.

Oort, A. H., and Rasmusson, E. M., 1974: Atmospheric circulation statistics, U.S. Dept. of Commerce, NOAA.

Palmen, E., and Newton, C. W., 1969: *Atmospheric Circulation System,* Academic Press, New York.

Pedlosky, J., 1979: *Geophysical Fluid Dynamics,* Springer-Verlag, pp 624.

Perry, J. S., 1967: Long wave energy processes in the 1963 sudden warming. *J. Atmos. Sci.*, **24,** 539–550.

Pfeffer, R. L., 1981: Wave–mean flow interaction in the atmosphere. *J. Atmos. Sci.*, **38,** 1340–1359.

Phillips, N. A., 1963: Geostrophic motions. *Rev. Geophys.*, **1,** 123–176.

Philpot, H. R., 1969: Antarctic stratospheric warming reviewed in the light of the 1967 observations. *Quart. J. Roy. Meteor. Soc.*, **95,** 329–348.

Romea, R. D., 1977: The effects of friction and on finite-amplitude baroclinic waves. *J. Atmos. Sci.*, **34,** 1689–1695.

Wallace, J. M. and Hobbs, P. V., 1977: *Atmospheric Science: An Introductory Survey,* Academic Press, 467 pp.

Wang, B., 1984: Generation and evolution of diabatic planetary waves in continuously stratified atmosphere with Ekman dissipation. Ph.D. dissertation, Florida State University.

——, and A. Barcilon, 1985: Atmospheric vacillation: The weakly Nonlinear dynamics of a planetary Green mode. *J. Atmos. Sci.*

Wiin-Nielsen, A., 1975: On large scale heating and atmospheric waves. *Proc. Seminar on Scientific foundation of medium-range weather forecasts.* Reading, (1975), p. 139–202.

Williams, G. P., and Robinson, J. B., 1974: Generalized Eady waves with Ekman pumping. *J. Atmos. Sci.*, **31,** 1768–1776.